Numerical modelling of distinct ice lenses in frost heave

Numerical modelling of distinct ice lenses in frost heave

S.A. Ghoreishian Amiri[1], G. Grimstad[1], H. Gao[1], S. Kjelstrup[2]

[1]PoreLab, Department of Civil and Environmental Engineering, Norwegian University of Science and Technology (NTNU), Trondheim, Norway.
[2]PoreLab, Department of Chemistry, Norwegian University of Science and Technology (NTNU), Trondheim, Norway.

corresponding author's e-mail: seyed.amiri@ntnu.no

Abstract. Frost heave happens when three conditions coincide: the temperature is below the normal freezing point of bulk water, the sub-cooled water is connected to a water reservoir, and the mechanical conditions of the soil allows the ice lens to grow. Upon further penetration of the freezing front, the relative permeability of the soil around the growing ice lens may dramatically decrease, and the ice lens stops growing. Then, if the three requirements for initiating a new ice lens coincide again, another ice lens will appear and start to grow. In this paper, a new thermo-hydro-mechanical (THM) model has been developed to capture the formation and growth of multiple ice lenses in a freezing ground. Non-equilibrium thermodynamic theory was used to derive the coupled transport equations of heat and mass. Fracture mechanics has been employed to handle the mechanical requirements for the position and growth of ice lens. The governing partial differential equations have been solved using the extended finite element method (X-FEM). In this method, the ice lens is treated as a kind of discontinuity inside the corresponding elements.
Keywords: Frost heave, Distinct ice lenses, THM model, X-FEM solution

1. Introduction

Frost heave is defined as the upwards movement of the ground surface due to formation of ice within fine-grained soils. It can potentially cause many engineering problems, like damage to pavements and foundation of structures. The phenomenon has been known for a long time [1] and has been the subject of numerous studies. A number of experimental investigations at various scales, from small-scale one-dimensional tests (e.g. [2, 3]) to large-scale three-dimensional cases (e.g. [4]), have been reported in literature. It has been recognized, through the experiments, that frost heave is much bigger than the molar volume expansion of freezing water. The phenomenon, actually, relates to the fact that in fine-grained soils, unfrozen water can exist at temperatures down to -70°C. This unfrozen water has a thermodynamic potential that causes the pore water to flow down temperature gradients.

Several studies have investigated the development of models to predict frost heave. In a series of papers, Konrad and Morgenstern [5-7] presented a theory of frost heave by introducing the segregation potential (SP) concept. However, the SP model has a semi-empirical nature and does not explicitly formulate the SP coefficient in terms of more fundamental soil properties like soil freezing characteristic curve. Other shortcomings of this theory are summarised by Nixon [8].

The key idea in the SP model was to connect the heave rate to temperature gradient. A similar idea was theoretically derived by [9, 10] using the theory of non-equilibrium thermodynamic. Their theoretical works resulted in a coupled transport equation of heat and mass within the frozen part of

the system. It implies that, in the frozen area, water will not only move due to a pressure gradient, but also, due to temperature gradient. The same conclusion was drawn by Gilpin [11] through experimental evidence. This idea was used by Nakano [12] to study the steady growth of a segregated ice layer in freezing soils. Later, Thomas *et al.* [13] developed a coupled THM model to describe the dynamic of ice lens formation and growth, based on the same idea.

O'Neill and Miller [14] introduced a rigid ice model for frost heave assuming pore ice motion by thermal regelation. Thermal regelation is known as a phenomenon that causes the isolated grains embedded in ice to move by a process of melting and refreezing. Similar idea has been followed by Rempel *et al.* [15] emphasizing more on the microscopic physics that drives the frost-heave process. This viewpoint does not necessarily contradict the former idea discussed in the previous paragraph.

In a more pragmatic approach, Nishimura *et al.* [16]; Zhang and Michalowski [17] and Ghoreishian Amiri *et al.* [18] tried to simulate the phenomenon by introducing a thermal triggering mechanism in their mechanical constitutive model. In this approach, as a result of freezing, the porous material will show a tendency of dilation (volume expansion). This demand from the material law will, in time, be responded by transport of water into the (partially) frozen area, and/or by a decrease in pore water pressure. This approach is popular among geotechnical engineers, since it is relatively easy to be implemented in the existing computational codes, and at the same time, is able to produce reasonable results. However, it does not follow the actual physic of the problem.

In this paper, a coupled THM model for simulating frost heave phenomenon is presented. In this model, the force equilibrium is incorporated with heat and mass balance equations, and a simple stress criterion for initiating new ice lensing is adopted. In terms of the driving forces of the phenomenon, it follows the approach presented by Førland and Kjelstrup Ratkje [9]; and Derjaguin and Churaev [10]; i.e. coupled transport of mass and heat. The finial governing partial differential equations of the system are solved using a version of X-FEM in the spatial domain, and a fully implicit finite difference scheme (FDM) in the time domain. The model is applied to simulate a small-scale column-freezing test, and reasonable agreement is achieved.

2. Conceptual model

According to Førland and Kjelstrup Ratkje [9] and Derjaguin and Churaev [10], the transport equations of heat and mass for frost heave yielded by non-equilibrium thermodynamic have the following form:

$$\boldsymbol{q}_w = -\frac{k_r K}{\mu_w}(\nabla p_w - \rho_w \boldsymbol{g}) - \alpha \frac{k_r K}{\mu_w}\frac{\rho_i l}{T}\nabla T \tag{1}$$

$$\boldsymbol{q}_H = -\alpha \frac{k_r K}{\mu_w}\rho_i l\ (\nabla p_w - \rho_w \boldsymbol{g}) - \left(\lambda_s^{1-n}.\lambda_w^{ns_w}.\lambda_i^{ns_i}\right)\nabla T \tag{2}$$

where q_w and q_H are the flux of mass and heat, respectively, p_w is the measurable water pressure, $\boldsymbol{g}$ denotes the gravity, T is temperature, K is the absolute permeability, μ_w is the dynamic viscosity of water, k_r denotes relative permeability for unfrozen water, l is the latent heat of fusion, λ_α is the thermal conductivity of each phase, and α is a parameter defined as:

$$\begin{cases} \alpha = 1 & T < T_0 \\ \alpha = 0 & T \geq T_0 \end{cases} \tag{3}$$

where T_0 is the freezing temperature of bulk water.

These coupled transport equations, together with the balance equations of mass and heat, are enough to describe the system at steady state with a predefined position of the ice lens. To describe the dynamic of the system, including initiation and growth of multiple ice lenses, we need to add the force equilibrium equation and define an appropriate stress measure and crack criterion.

To describe the concept of the model, we can consider a one-dimensional saturated, solute-free soil-column subjected to a freezing temperature from the top boundary (Fig. 1-a). According to Eq. (1), the

temperature gradient in the frozen fringe results in a mass flux term towards the frozen fringe. However, due to stiffness of the soil and the force equilibrium requirement, this mass flux term will be (partially) cancelled, and consequently, the pore water pressure will develop in that zone. The pore water pressure will in turn decrease the effective stress, and at some point, a (tensile) crack might appear (Fig. 1-b). From this point, water can freely migrate to the cracked zone and the ice lens will start growing (Fig 1-c). More penetration of the freezing front will result in a dramatic decrease of the relative permeability around the ice lens, and consequently the ice lens will stop growing (Fig. 1-d). Then, the same scenario might happen around the new freezing front. The pore water pressure will increase again and might result in a new crack (Fig. 1-e) and new active ice lens (Fig. 1-f).

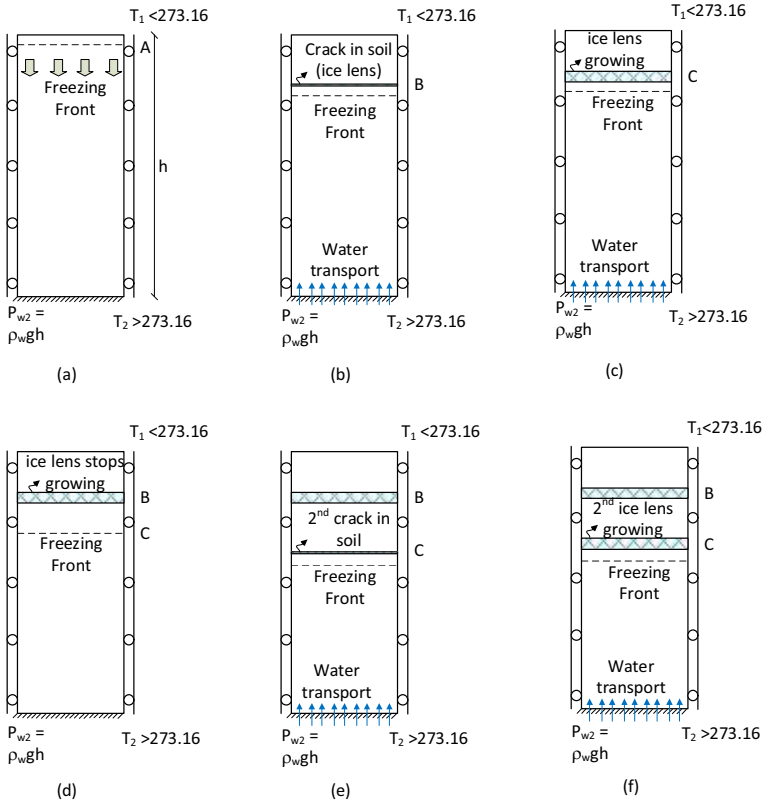

Figure 1. Formation of multiple ice lenses in soil column

3. Governing Equations

The system of concern, in this paper, is a mixture of a deformable porous medium saturated with ice and unfrozen water. The system is described as the superposition of all phases.

In deriving the balance equations, it is assumed that the ice phase has a similar motion of the solid skeleton. Thus, the Lagrangian form is used for the ice phase and the solid skeleton, while motion of the unfrozen water phase is described relative to the motion of the solid skeleton (or ice phase), i.e. the Eulerian form of the balance equations with respect to the motion of the solid skeleton are used for the unfrozen water phase.

Note that throughout this paper, compressive stress and strain are assumed to be positive.

3.1. Continuity

The mass balance equation for water and ice phases can be written as:

$$n\left(\rho_w-\rho_i\right)\dot{s}_w+\nabla.\left(\rho_w\boldsymbol{q}_w\right)-\left(s_w\rho_w+s_i\rho_i\right)\dot{\varepsilon}_v=0 \tag{4}$$

where n is the porosity, ρ_w is water density, ρ_i denotes ice density, s_w is the unfrozen water saturation, s_i is ice saturation and ε_v denoted the volumetric strain. Substituting Eq. (1) into Eq. (4) results in the final form of the continuity equation:

$$n(\rho_w-\rho_i)\dot{s}_w-\nabla.\left[\frac{k_r K}{\mu_w}\rho_w(\nabla p_w-\rho_w \boldsymbol{g})\right]-\nabla.\left[\alpha\frac{k_r K}{\mu_w}\frac{\rho_i l}{T}\rho_w\nabla T\right]-(s_w\rho_w+s_i\rho_i)\dot{\varepsilon}_v=0 \quad (5)$$

Referring to Watanabe and Osada [19], the relative permeability for unfrozen water can be estimated from that of unsaturated soil based on the liquid (unfrozen) water saturation. Thus, the model proposed by van Genuchten [20] for estimating the relative permeability in unsaturated soil might be used here for frozen soil:

$$k_r=\sqrt{s_w}\left[1-\left(1-s_w^{1/\lambda}\right)^{\lambda}\right]^2 \quad (6)$$

where λ is a model parameter.

Referring to Kurylyk and Watanabe [21], the unfrozen water saturation; i.e. the freezing characteristic curve, might be formulated based on the pressure difference between ice and water phase. Considering the Clapeyron equation as the basis for the pressure difference between ice and water phases, the following mathematical relation can be used here [20]:

$$s_w=\left[1+\left(\frac{S_{cry}}{\rho_r}\right)^{1/(1-\lambda)}\right]^{-\lambda} \quad (7)$$

where S_{cry} is the cryogenic suction, ρ_r and λ are model parameters. The cryogenic suction is calculated based on Clapeyron equation [22]:

$$S_{cry}=p_i-p_w\simeq-\rho_i l\ln\frac{T}{T_0} \quad (8)$$

3.2. Heat transfer

By enforcing the local thermal equilibrium, a single energy balance equation can be used to describe the heat transfer process in a multiphase system. This assumption implies that all the phases at each spatial point reach thermal equilibrium instantaneously together.

Neglecting the kinetic energy, viscous and intrinsic dissipation, the energy balance on an infinitesimal multiphase element can be written as

$$(\rho C)_{\text{eff}}\dot{T}+(\rho_w C_w\boldsymbol{q}_w).\nabla T+\nabla.\boldsymbol{q}_H-l.\dot{m}_{w\to i}=0 \quad (9)$$

where $(\rho C)_{\text{eff}}$ is the effective heat capacity of the mixture that can be calculated as

$$(\rho C)_{\text{eff}}=(1-n)\rho_s C_s+ns_w\rho_w C_w+ns_i\rho_i C_i \quad (10)$$

where λ_α is the thermal conductivity of the phase α. The last term in Eq. (9) is standing for the phase change from water to ice. To find this term, we need to write the mass balance equation of the ice phase:

$$-n\rho_i\dot{s}_w-s_i\rho_i\dot{\varepsilon}_v-\dot{m}_{w\to i}=0\Rightarrow\dot{m}_{w\to i}=-n\rho_i\dot{s}_w-s_i\rho_i\dot{\varepsilon}_v \quad (11)$$

Substituting Eq. (2) into Eq. (9) results in the final form of the heat transfer equation:

$$(\rho C)_{\text{eff}}\dot{T}+(\rho_w C_w\boldsymbol{q}_w).\nabla T-\nabla.\left[\alpha\frac{k_r K}{\mu_w}\rho_i l\ (\nabla p_w-\rho_w\boldsymbol{g})\right]-\nabla.\left[\left(\lambda_s^{1-n}.\lambda_w^{ns_w}.\lambda_i^{ns_i}\right)\nabla T\right]-l.\dot{m}_{w\to i}=0 \quad (12)$$

3.3. Force equilibrium

The force equilibrium of the system can be written as:

$$\nabla.\boldsymbol{\sigma} - \rho \boldsymbol{g} = 0 \tag{13}$$

where $\boldsymbol{\sigma}$ is the total stress, and ρ is the density of the mixture:

$$\rho = (1-n)\rho_s + ns_w\rho_w + ns_i\rho_i \tag{14}$$

The total stress can be additively decomposed into the normalized water pressure and solid phase stress:

$$\boldsymbol{\sigma} = \boldsymbol{\sigma}^* + p_w \boldsymbol{I} \tag{15}$$

where $\boldsymbol{\sigma}^*$ is the solid phase stress defined as the combined stress of soil grains and ice, and $\boldsymbol{I}$ is the unit tensor. The solid phase stress is considered as the part of the total stress which is responsible for the mechanical deformation of the system. We need to have a constitutive model connecting the mechanical deformation/strain to the solid phase stress. In this stage, we follow a simple elastic constitutive model with a simple 1D crack criterion:

$$d\boldsymbol{\sigma}^* = \boldsymbol{D}^e.d\boldsymbol{\varepsilon} \tag{16}$$

$$F = -\sigma^*_n - a = 0 \tag{17}$$

where $\boldsymbol{D}^e$ is the elastic stiffness tensor, F is the crack criterion and a is the maximum effect of ice cementation at the fully frozen state. Note that the cementation effect will immediately disappear after the crack.

The following paragraph summarize the idea behind the presented formulation:

When a soil sample subjects to freeze, according to the second term in Eq. (1), water tends to come into the frozen fringe. However, at the beginning, it can't segregate the grains to provide a new volume for transport. So that, the pore water pressure will increase to provide a pressure gradient (the first term in Eq. (1)) to cancel the water flux due to temperature gradient. This results in a decrease in solid phase stress, and at some point, the solid phase stress will be small enough to create a crack.

4. Numerical solution

Considering the discontinuity imposed by ice lenses, the extended finite element method is employed for spatial discretization. In this approach, the ice lens is considered as a discontinuity (crack) in the soil body. The discontinuity is not generally free to expand, but it is free to expand in response to thermal induced water flux.

In order to discretize the governing equations, the primary unknown variables (i.e. displacement, pore water pressure and temperature) should be approximated using appropriate shape functions. In the X-FE method, the conventional FE shape functions are locally enriched using proper enrichment functions based on the type of the discontinuity.

The ice lens growth requires a discontinuous displacement field in the normal direction to the crack (strong discontinuity). Indeed, the mass and heat transfer imply the fluid and heat flux, in the normal direction to the crack, to be also discontinuous, while the pressure and temperature fields are continuous (weak discontinuity). In the context of X-FEM, strong discontinuities are approximated by adding a discontinuous enrichment function to the corresponding standard approximated space. While, weak discontinuities are taken into account by adding a continuous enrichment function with discontinuous gradient. In this case, we use a type of Heaviside and level-set functions to model the strong and weak discontinuities over the crack interface, respectively:

$$\boldsymbol{u}(\boldsymbol{x},t) = \sum_{i=1}^{\mathfrak{N}} N_{u_i}(\boldsymbol{\xi})\hat{\boldsymbol{u}}_i(t) + \sum_{j=1}^{\mathfrak{M}} \left[\overline{N}_{u_j}(\boldsymbol{\xi}) \left(H(\varphi(\boldsymbol{\xi})) - H(\varphi(\boldsymbol{\xi}_j)) \right) \boldsymbol{n}_{\Gamma_d} \right] \hat{a}_j(t) = \boldsymbol{N}_u^{std}\hat{\boldsymbol{u}} + \boldsymbol{N}_u^{enr}\boldsymbol{L}\hat{\boldsymbol{a}} \tag{18}$$

$$p_w(\boldsymbol{x},t)=\sum_{i=1}^{\mathfrak{N}}N_{p_i}(\boldsymbol{\xi})\hat{p}_{w_i}(t)+\sum_{j=1}^{\mathfrak{M}}\bar{N}_{p_j}(\boldsymbol{\xi})\psi_p(\boldsymbol{\xi})\hat{b}_j(t)=\boldsymbol{N}_p^{std}\hat{\boldsymbol{p}}_w+\boldsymbol{N}_p^{enr}\hat{\boldsymbol{b}} \tag{19}$$

$$T(\boldsymbol{x},t)=\sum_{i=1}^{\mathfrak{N}}N_{T_i}(\boldsymbol{\xi})\hat{T}_i(t)+\sum_{j=1}^{\mathfrak{M}}\bar{N}_{T_j}(\boldsymbol{\xi})\psi_T(\boldsymbol{\xi})\hat{c}_j(t)=\boldsymbol{N}_T^{std}\hat{\boldsymbol{T}}+\boldsymbol{N}_T^{enr}\hat{\boldsymbol{c}} \tag{20}$$

where $\boldsymbol{\xi}$ is the natural coordinate system of the element, $\mathfrak{N}$ is the set of all nodes, $\mathfrak{M}$ is the set of enriched nodes, $N(\boldsymbol{\xi})$ and $\bar{N}(\boldsymbol{\xi})$ are the standard FEM shape functions for the field variable in its standard and enriched parts, respectively; $\hat{\boldsymbol{u}}$, $\hat{\boldsymbol{p}}_w$ and $\hat{\boldsymbol{T}}$ are the nodal displacement, pore pressure and temperature, respectively; $\boldsymbol{L}$ is the transformation matrix; $\hat{\boldsymbol{a}}$, $\hat{\boldsymbol{b}}$ and $\hat{\boldsymbol{c}}$ are the enhanced nodal degree of freedom for deformation, pressure and temperature, respectively; $H(\varphi(\boldsymbol{\xi}))$ is the Heaviside function defined in (21), and $\psi(\boldsymbol{\xi})$ is the modified level-set function defined in (22).

$$H(\varphi(\boldsymbol{\xi}))=\begin{cases}+1 & \varphi(\boldsymbol{\xi})\geq 0\\ 0 & \varphi(\boldsymbol{\xi})<0\end{cases} \tag{21}$$

$$\psi_\alpha(\boldsymbol{\xi})=\sum_{k=1}^{\mathfrak{M}}\bar{N}_{\alpha_k}(\boldsymbol{\xi})\left|\varphi(\boldsymbol{\xi}_k)\right|-\left|\sum_{k=1}^{\mathfrak{M}}\bar{N}_{\alpha_k}(\boldsymbol{\xi})\varphi(\boldsymbol{\xi}_k)\right| \quad ;\ \alpha=p,T \tag{22}$$

where $\varphi(\boldsymbol{\xi})$ is the signed distance function defined based on the absolute value of the level set function as

$$\varphi(\boldsymbol{\xi})=\left\|\boldsymbol{\xi}-\boldsymbol{\xi}_{\Gamma_d}\right\|\operatorname{sign}\left((\boldsymbol{\xi}-\boldsymbol{\xi}_{\Gamma_d}).\boldsymbol{n}_{\Gamma_d}\right) \tag{23}$$

where $\boldsymbol{\xi}_{\Gamma_d}$ is the closest point projection of $\boldsymbol{\xi}$ onto the discontinuity interface, and $\|\ \|$ denotes the Euclidean norm; accordingly $\left\|\boldsymbol{\xi}-\boldsymbol{\xi}_{\Gamma_d}\right\|$ specifies the distance of point $\boldsymbol{\xi}$ to the discontinuity.

The application of the extended finite element method results in the following semi-discrete equation:

$$\boldsymbol{A}\frac{d\boldsymbol{X}}{dt}+\boldsymbol{B}\boldsymbol{X}=\boldsymbol{f}^{\text{ext}}+\boldsymbol{f}^{\text{int}} \tag{24}$$

where $\boldsymbol{X}$ is the solution vector, $\boldsymbol{f}^{\text{ext}}$ is the prescribe nodal forces/fluxes, and $\boldsymbol{f}^{\text{int}}$ denotes the interactions between the crack and porous medium.

The time discretization of the equation is performed by a fully implicit first-order accurate finite difference scheme:

$$\left[\boldsymbol{A}+\Delta t\boldsymbol{B}\right]_{t+1}\boldsymbol{X}_{t+1}=\Delta t\left(\boldsymbol{f}^{\text{ext}}\right)_{t+1}+\Delta t\left(\boldsymbol{f}^{\text{int}}\right)_{t+1}+\boldsymbol{A}_{t+1}\boldsymbol{X}_t \tag{25}$$

The nonlinear equation (25) is solved using Newton-Raphson iterative algorithm:

$$\mathbb{J}_{t+1}^{i}.\Delta\boldsymbol{X}_{t+1}^{i+1}=-\mathbb{R}_{t+1}^{i} \tag{26}$$

where

$$\mathbb{J}_{t+1}^{i}=\left[\boldsymbol{A}+\Delta t\boldsymbol{B}\right]_{t+1}^{i}-\Delta t\frac{\partial\left(\boldsymbol{f}^{\text{int}}\right)_{t+1}^{i}}{\partial\boldsymbol{X}} \tag{27}$$

$$\Delta\boldsymbol{X}_{t+1}^{i+1}=\boldsymbol{X}_{t+1}^{i+1}-\boldsymbol{X}_{t+1}^{i} \tag{28}$$

$$\mathbb{R}_{t+1}^{i}=\left[\boldsymbol{A}+\Delta t\boldsymbol{B}\right]_{t+1}^{i}\boldsymbol{X}_{t+1}-\Delta t\left(\boldsymbol{f}^{\text{ext}}\right)_{t+1}-\Delta t\left(\boldsymbol{f}^{\text{int}}\right)_{t+1}^{i}-\boldsymbol{A}_{t+1}^{i}\boldsymbol{X}_t \tag{29}$$

5. Numerical Example

The proposed model is verified by simulating a small-scale one-dimensional freezing test on Devon silt, reported by Konrad and Morgenstern [5, 6]. The soil sample was initially unfrozen, with a temperature of +3°C. The top surface temperature was then reduced to -5.5°C to trigger the freezing process, and remained constant during the test. Water was freely available at the base, at zero pressure. The initial porosity of the 78 mm soil sample was 38%. The hydraulic conductivity of the unfrozen soil was 1×10^{-7} cm/s, and the soil freezing characteristic curve is given in Fig. 2. The heat capacity and thermal conductivity of the constituents were not reported in [5, 6]. We used typical values, listed in table 1, for these parameters. Mechanical parameters are also listed in the table.

In the simulation, the sample was discretized using 200 one-dimensional elements, without any prescribed crack. As described in Fig. 1, at the beginning of the simulation, pore water pressure developed around the frozen fringe to (partially) cancel the temperature induced water flux (i.e. the second term in equation (1)). This in turn decreased the effective stress until the crack criterion, equation (17), was satisfied for the first time. From this point, the corresponding element was enriched, and water freely migrated to the crack. More penetration of the freezing front resulted in a dramatic decrease of the relative permeability, equation (6), around the ice lens, and consequently the ice lens stopped growing. This scenario was repeated until the crack criterion is exceeded nowhere else.

Table 1. Additional parameters for Devon silt

Parameter	Value
Heat capacity of soil grains	2095 J/kg K
Heat capacity of ice	4190 J/kg K
Heat capacity of water	900 J/kg K
Ther. Cond. of soil grains	3 J/m s K
Ther. Cond. of ice	2.2 J/m s K
Ther. Cond. of water	0.6 J/m s K
Young's modulus	5 MPa
Poisson's ratio	0.25
Crack criterion	0.2 MPa

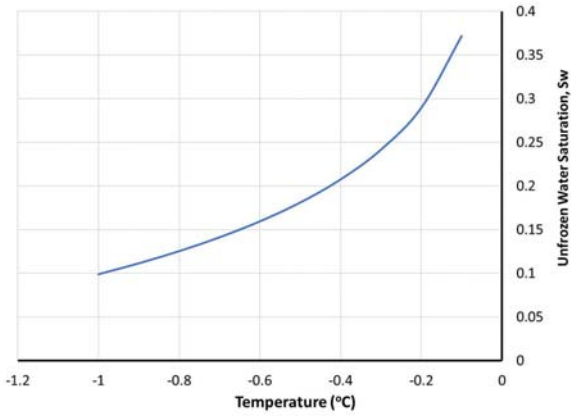

Figure 2. Soil freezing characteristic curve for Devon silt [23]

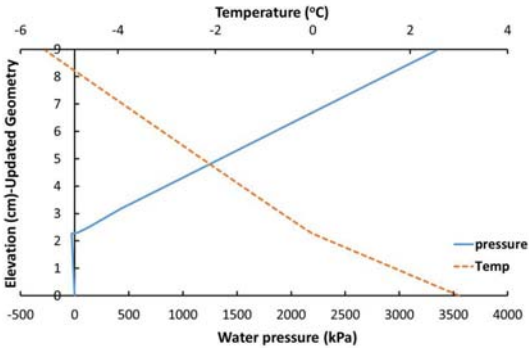

Figure 3. Temperature and pore pressure profile after 44 hrs

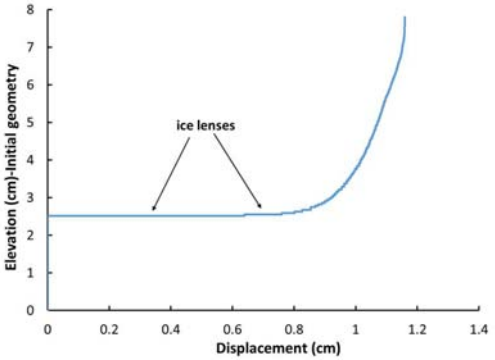

Figure 4. Displacement profile after 44 hrs

The pore water pressure and temperature profiles are shown in Fig. 3, on the updated geometry of the column. Below the freezing front, a suction of around 27 kPa has been predicted by the model. This suction value is in the range of those reported on Devon silt [23]. Fig. 4 shows the displacement field. As shown in the figure, the final ice lens is predicted to be at 25 mm from the base. The temperature at the base of the last ice lens is calculated as -0.5°C. These values are reported by Konrad and Morgenstern [6] as 28 mm and -0.16°C, respectively. Fig. 5 compares the calculated and measured frost heave (water in-take) in time, and reasonable agreement is achieved.

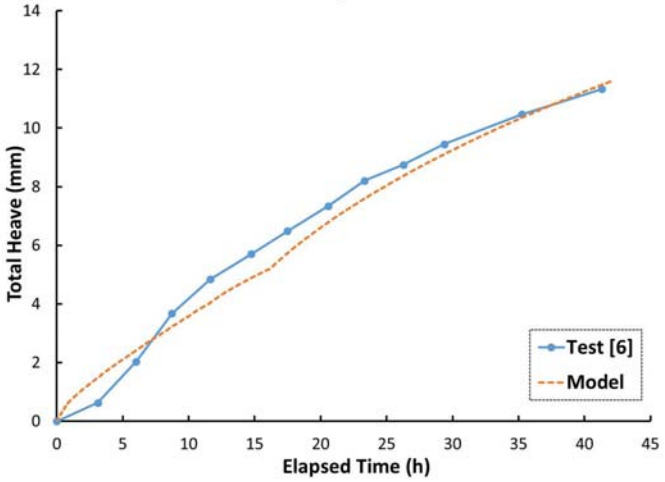

Figure 5. Comparison between the measured and predicted frost heave

6. Conclusion

This paper presents a THM model describing the initiation and growth of multiple ice lenses in soil freezing. Based on the theory of non-equilibrium thermodynamic, temperature gradient is the main driving force of frost heave phenomenon. It results in a coupled transport equation of mass and heat. This coupled transport equation, together with the mass and energy balance equations are, generally, enough to fully describe the frost heave phenomenon at steady state. To describe the dynamic of the system, the force equilibrium equation, appropriate stress measure and crack criterion are also introduced. The governing equations are solved using the extended finite element method (X-FEM). In this method, the ice lens is treated as a kind of discontinuity inside the corresponding elements. The model is applied to simulate a small-scale column-freezing test, and reasonable agreement is achieved. For broader applications, the two-dimensional version of the model is currently under development, and will follow in upcoming works.

Acknowledgments

This work is supported by the Research council of Norway through its Centers of Excellence funding Scheme, project number 262644.

7. References

[1]. Taber S. Frost Heaving. The Journal of Geology. 1929;37(5):428-61.
[2]. Penner E. Aspects of ice lens growth in soils. Cold Regions Science and Technology. 1986;13(1):91-100.
[3]. Konrad JM. Frost heave Mechanics. Edmonton, Alberta: The Univ. Alberta; 1980.
[4]. Williams PJ, Riseborough DW, Smith MW. The France-Canada Joint Study Of Deformation Of An Experimental Pipe Line By Differential Frost Heave. ISOPE-93-03-1-056. 1993;3(01):5.
[5]. Konrad J-M, Morgenstern NR. A mechanistic theory of ice lens formation in fine-grained soils. Canadian Geotechnical Journal. 1980;17(4):473-86.

[6]. Konrad J-M, Morgenstern NR. The segregation potential of a freezing soil. Canadian Geotechnical Journal. 1981;18(4):482-91.
[7]. Konrad JM, Morgenstern NR. Prediction of frost heave in the laboratory during transient freezing. Canadian Geotechnical Journal. 1982;19(3):250-9.
[8]. Nixon JF. Discrete ice lens theory for frost heave in soils. Canadian Geotechnical Journal. 1991;28(6):843-59.
[9]. Førland T, Kjelstrup Ratkje S. Irreversible thermodynamic treatment of frost heave. Engineering Geology. 1981;18(1):225-9.
[10]. Derjaguin BV, Churaev NV. Flow of nonfreezing water interlayers and frost heaving. Progress in Surface Science. 1993;43(1):232-40.
[11]. Gilpin RR. A model for the prediction of ice lensing and frost heave in soils. Water Resources Research. 1980;16(5):918-30.
[12]. Nakano Y. Quasi-steady problems in freezing soils: I. Analysis on the steady growth of an ice layer. Cold Regions Science and Technology. 1990;17(3):207-26.
[13]. Thomas HR, Harris C, Cleall P, Kern-Luetschg M, Li YC. Modelling of cryogenic processes in permafrost and seasonally frozen soils. Géotechnique. 2009;59(3):173-84.
[14]. O'Neill K, Miller RD. Exploration of a Rigid Ice Model of Frost Heave. Water Resources Research. 1985;21(3):281-96.
[15]. Rempel AW, Wettlaufer JS, Worster MG. Premelting dynamics in a continuum model of frost heave. Journal of Fluid Mechanics. 2004;498:227-44.
[16]. Nishimura S, Gens A, Jardine RJ, Olivella S. THM-coupled finite element analysis of frozen soil: formulation and application. Géotechnique. 2009;59(3):159-71.
[17]. Zhang Y, Michalowski RL. Thermal-Hydro-Mechanical Analysis of Frost Heave and Thaw Settlement. Journal of Geotechnical and Geoenvironmental Engineering. 2015;141(7):04015027.
[18]. Ghoreishian Amiri SA, Grimstad G, Aukenthaler M, Panagoulias M, Brinkgreve RBJ, Haxaire A. The frozen and unfrozen soil model. Delft: Technical report – PALXIS bv; 2016.
[19]. Watanabe K, Osada Y. Comparison of Hydraulic Conductivity in Frozen Saturated and Unfrozen Unsaturated Soils. Vadose Zone Journal. 2016;15(5).
[20]. van Genuchten MT. A Closed-form Equation for Predicting the Hydraulic Conductivity of Unsaturated Soils1. Soil Science Society of America Journal. 1980;44:892-8.
[21]. Kurylyk BL, Watanabe K. The mathematical representation of freezing and thawing processes in variably-saturated, non-deformable soils. Advances in Water Resources. 2013;60:160-77.
[22]. Wettlaufer JS, Worster MG. Premelting dynamics. Annual Review of Fluid Mechanics. 2006;38(1):427-52.
[23]. Konrad J-M, Duquennoi C. A model for water transport and ice lensing in freezing soils. Water Resources Research. 1993;29(9):3109-24.